Surface & Coatings Technology 313 (2017) 136–142

Contents lists available at ScienceDirect

Surface & Coatings Technology

journal homepage: www.elsevier.com/locate/surfcoat

Estimation of microstructure and corrosion properties of peened nickel aluminum bronze

Chengxi Wang [a], Chuanhai Jiang [a,*], Ze Chai [a], Ming Chen [a], Lianbo Wang [a], Vincent Ji [b]

[a] School of Materials Science and Engineering, Shanghai Jiao Tong University, No. 800, Dongchuan Road, Shanghai 200240, PR China
[b] LEMHE/ICMMO, UMR 8182, Université Paris-Sud 11, 91405 Orsay, France

ARTICLE INFO

Article history:
Received 17 September 2016
Revised 18 January 2017
Accepted in revised form 20 January 2017
Available online 21 January 2017

Keywords:
Corrosion resistance
Microstructure
Residual stress
Shot peening
Nickel aluminum bronze

ABSTRACT

In this study, the effects of shot peening on the residual stress, microstructure and corrosion properties of nickel aluminum bronze were evaluated by using X-ray stress analyzer, X-ray diffraction profile analysis, transmission electron microscopy and electrochemical tests. Shot peening improved the hardness and compressive residual stress of the surface layer. A thin layer of nanometer-scaled domain formed at the top surface and the domain size raised constantly with depth until it reached nearly the value of matrix. The micro-strain and dislocation density dropped gradually with the increasing distance toward interior. Moreover, the samples treated by shot peening with different intensities all showed superior corrosion resistance than that of unpeened ones. However, further improving the peening density resulted in a poor corrosion performance, which was mostly ascribed to the increased surface roughness due to the raised deformation.

1. Introduction

Nickel aluminum bronzes (NAB) are widely used in components ranging from seawater pumps, valves and propellers to landing gear bearings and bushings due to their unique combination of high strength, good damping capacity, and excellent wear and corrosion resistance [1]. However, these alloys are often subjected to selective phase corrosion and stress corrosion cracking when working in seawater or other extreme conditions [2] due to their complex phases and inhomogeneous distribution of residual stresses.

In most cases, the surface is more likely to be failure than the central part. Hence a number of studies have been carried out recently to enhance the surface mechanical properties and corrosion resistance of NAB alloy. For instance, DR Ni et al. improved the corrosion resistance of cast NAB by using friction stir processing to refine the coarse microstructure [3]; K.D. Klassen et al. reported the passivation film formed at the surface of laser cladding treated NAB [4]. In comparison, shot peening (SP) as one of the mostly used methods to improve the surface properties of components, can simultaneously refine the microstructure and induce the compressive residual stress into the surface layers. However, enhancing the surface of NAB alloys by SP has not enough been studied since many investigations indicated the conflicting results about the effect of SP treatment on the corrosion performance in other alloys. Han-sang Lee reported that the 304 stainless steel treated by traditional SP showed the lowest corrosion resistance in comparison with the matrix or the ultrasonic peening treated ones, and accounted it mainly for the surface roughness [5]. X.Y. Wang demonstrated that the sandblasting deteriorated the corrosion resistance of 304 stainless steel, and only the subsequent annealing could make it superior than the as-received one [6]. Trdan Uroš et al. published that the laser peening enabled the pitting potential of 6082 aluminum alloy shift to more positive, which ensured its higher corrosion resistance [7]. Omar Hatamleh et al. also founded that the shot peened surface of friction stir welded aluminum alloy joint has fewer pits than the unpeened one [8]. So the present study is attempt to investigate the modification of surface properties of NAB alloy after SP treatment.

2. Experiments

C63020 NAB alloy with the chemical composition listed in Table 1 was employed in this work. It was non-vacuum melted and followed by forging at 850 °C, then the specimens with effective dimensions of 20 mm × 10 mm × 10 mm were cut from the block sample by electro-discharge cutting. Table 2 showed the mechanical properties of the specimen. All samples were divided into three groups and ground to 1000-grit SiC before SP treatment and other subsequent tests. The untreated group was used as reference for comparing with other groups subjected to SP with different intensities. A traditional air blast machine (Carthing Machinery Company, Shanghai) was employed to carry out the peening treatment. The shot medium was ZrO_2 ceramic beads with average diameter of 0.25 mm and the stand-off distance was 100 mm. The different intensities of 0.10 and 0.15 mmA, which were

* Corresponding author.
E-mail address: chjsjtu@163.com (C. Jiang).

http://dx.doi.org/10.1016/j.surfcoat.2017.01.073
0257-8972/

Table 1
Chemical composition of the NAB alloy used in the present study.

Elements (wt.%)	Al	Fe	Ni	Mn	Cu
C63020	10.06	4.02	3.63	0.25	Balanced

Table 2
Mechanical properties of the NAB alloy used in the present study.

Specimen	Yield strength (MPa)	Tensile strength (MPa)	Elongation (%)	Hardness (HV)
C63020	285	600	6	248

confirmed by A-type Almen test strips, were obtained under air pressures of 0.3 and 0.4 MPa, respectively. The coverage of all peened samples were ensured no less than 100%.

Optical microscopy (Axio Lab. A1, Carl Zeiss) and 3D non-contact Optical Surface Profiler (Zegate, Zygo) were employed to examine the changes of surface microstructure and surface roughness after SP treatment. The etchant was 5 g $FeCl_3$ + 2 mL HCl + 95 mL C_2H_5OH. The detailed microstructure was observed by TEM (JEM-2100F) working at 200 kV. TEM samples were first grounded to 70 μm using sand paper and subsequent twin-jet electro-polished in a mixture of 5 vol.% perchloric acid and 95 vol.% ethanol at −45 °C. XRD patterns were detected by Rigaku Ultima IV X-ray diffractometer (Cu-Kα radiation, 40 kV, 30 mA), scanning speed of 2°/min and a step of 0.01°, to evaluate the microstructure through line profile analysis. The residual stress information was collected by X-ray stress analyzer (LXRD, Proto, Canada, Cu-Kα radiation, 30 kV, 25 mA) and calculated using $\sin^2\psi$ method. Ni filter was selected and the shift of Cu (420) diffraction profile was detected during the measurement. The elastic constants S_1, $1/2S_2$ of Cu (420) were −3.11 and 11.72×10^{-6} MPa^{-1}, respectively. The surface Vickers hardnesses of samples with and without SP were measured by Digital Microhardness Tester (DHV-1000, Beijing), with the loading force of 1.98 N and the holding time of 15 s. The average value of five random points measured for each layer was determined as the final result. In order to investigate the variations of XRD patterns, residual stresses and micro-hardness along the depth, the samples were carefully etched using local electrochemical corrosion method layer by layer. NaCl saturation solution was used as electrolyte.

Electrochemical impedance spectroscopy (EIS) and polarization measurement were performed on CHI 660E electrochemical workstation(Chenhua, Shanghai). A saturated calomel electrode (SCE) was used as reference electrode, and a platinum sheet as auxiliary electrode. The corrosion medium was 3.5 wt% NaCl solution. Test samples were cut from plates and embedded in epoxy resin to ensure the exposing area of 1 cm^2 before being ultrasonic cleaned with acetone. All electrochemical measurements were carried out at room temperature, and the untreated sample was also tested as a reference. In order to reach the equilibrium potential, all samples were immersed into the corrosion medium for 1 h. Three samples of each groups were examined to ensure repeatability. During the potentiodynamic polarization curves measurement, the potential was set ranging from −500 to 1200 mV at a scan speed of 0.5 mV/s. EIS was performed in a frequency ranging from 100 KHz to 0.01 Hz with AC amplitude of ±10 mV superimposed to the open circuit potential value. In addition, the ZSimpwin software was employed to fit the experiments and data.

During X-ray diffraction line profile analysis, Materials Analysis Using Diffraction (MAUD) software [9]based on the Rietveld method was used to fit the whole XRD patterns, and the wildly used pseudo-Voigt function was adopted to resolve the broadened profiles due to variations of the coherently scattering domain (hereafter referred to as domain) size and the micro-strain. In this study, the POPA model [10] was introduced to analyze the average domain size and the micro-strain of Cu (111) lattice planes. In POPA model, the crystallite size (R) and the strain (ε) for cubic crystal system can be shown as follows:

$$\langle R_h \rangle = R_0 + R_1 K_4^1(x,\varphi) + R_2 K_6^1(x,\varphi) + \cdots \tag{1}$$

$$\langle \varepsilon_{hh}^2 \rangle E_H^4 = E_1\left(h^4 + k^4 + l^4\right) + 2E_2\left(h^2k^2 + k^2l^2 + l^2h^2\right) \tag{2}$$

where $\langle R_h \rangle$ is radius of the average crystallite, which denotes the domain size in the present study, $\langle \varepsilon_{hh} \rangle$ is the (h, k, l)-dependent strain, the right side of Eq. (1) is a convergent series of symmetrized spherical harmonics, E_1 and E_2 are the optimizable parameters, and h, k, l are the indices of crystal plane. During the fitting process, these parameters were optimized constantly until the calculated results coincided well enough with the experimental data. Weighted residual error R_{wp} as well as expected error R_{exp} and sig ($sig = R_{wp}/R_{exp}$) were recorded to characterize the fitting quality.

3. Results

3.1. Surface morphology

The cross-section metallographs of the NAB alloy before and after SP treatment were shown in Fig. 1(a) and (b). It is observable that the microstructure of C63020 mainly consists the Cu-rich solid solution α phase, some portion of retained β (β') and κ_{iv} phases, which are the

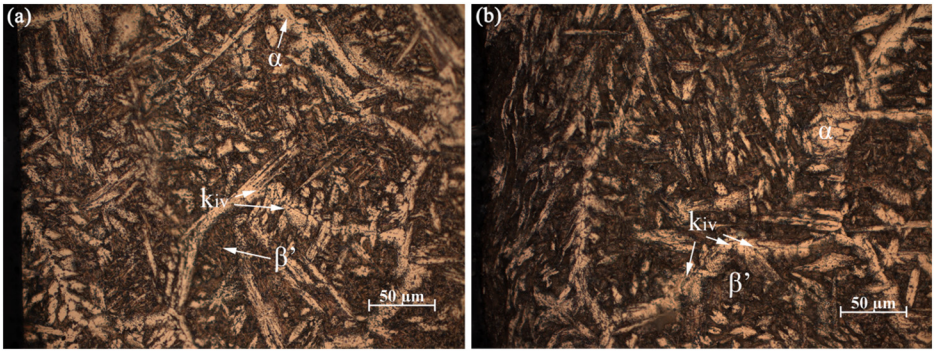

Fig. 1. Cross-section metallographs of NAB alloy before (a) and after (b) SP treatment (0.15 mmA). The left side is SP direction.